PFC/JA-82-32

OPTIMIZATION AND MONTE CARLO MODELING OF BUNDLE DIVERTORS*

T. F. Yang, A. Wan, R. Potok, D. T. Blackfield

Plasma Fusion Center
Massachusetts Institute of Technology
Cambridge, Massachusetts 02139 USA

*This work has been supported by the US Department of Energy Cont.#DE-AC02-78ET-51013.

OPTIMIZATION AND MONTE CARLO MODELING OF BUNDLE DIVERTORS

T. F. Yang, A. Wan, R. Potok, D. T. Blackfield

ABSTRACT

This paper describes a Monte Carlo study of the thermal conductivity and impurity transport in a tokamak with an optimized bundle divertor configuration. This configuration has been designed to obtain the best plasma performance. When collisions and electric fields are included, the thermal conductivity was found to be 40% larger than that of an axisymmetric neoclassical value. Without a divertor the oxygen impurity was found to diffuse towards the center of the plasma as predicted theoretically. However, this impurity diffused outwardly when the divertor was turned on. Few impurity particles diffused into the plasma when launched in the scrape-off layer. This optimized bundle divertor meets the engineering constraints of a power producing reactor.

1. INTRODUCTION

A bundle divertor [1,2] is a set of coils which creates a separatrix on the toroidal magnetic field of a tokamak and diverts a bundle of field lines from the outer layer of the plasma into a separate divertor chamber. In contrast to a poloidal divertor, the toroidal symmetry of the plasma is destroyed. This perturbation creates a localized magnetic field ripple and poses many problems in plasma confinement and tokamak engineering.

From the confinement point of view, the localized ripple may induce ergodicity of the magnetic surfaces, enhance the diffusive loss of thermal particles, and enhance the direct loss of energetic particles. The purpose of this paper is to study these effects and to find a way to minimize them. From the engineering point of view, a very large localized current is needed to produce a separatrix with strong toroidal magnetic field. This results in very large magnetic forces. The space available for the conductor and neutron shielding is limited due to competing effects of reducing the current density in the conductor and the perturbation on the toroidal field. These reactor technology problems are addressed later.

Aside from the physics and engineering questions mentioned above, the bundle divertor has many advantages: (1) Because the bundle divertor is a local appendage, a specific design is possible such that the divertor can be decoupled from the remainder of the tokamak system; (2) Substantial reductions may be achieved in the size of both toroidal and poloidal field coil sets; (3) The divertor chamber can be isolated from the main chamber to a much greater extent than the poloidal divertor chamber. This opens the way for more advanced energy and particle exhaust systems [3,4,5]; (4) The bundle divertor separatrix is fixed relative to the first wall and divertor coils can be operated in steady state. The first wall is therefore protected during start-up, shut-down, and disruptions. It is impprtant to understand the nature of the bundle divertor and find a method to optimize a design because of these advantages.

The most difficult engineering constraints are the current density in the conductor and shielding requirement. From practical experience 3 to 4 kA/cm^2 of current density is considered to be acceptable for both normal conductor and superconductor. The neutron shielding design study has shown that for a composite shielding material of tungsten and borated water of 60 cm thickness,

the lifetime can be longer than 2 MW-yr/m^2 for insulation materials tested in the dose limit of 10^7 to 10^9 Grays [6]. Therefore, a current density of 3.5 kA/cm^2 and shielding space of 60 cm are used as the engineering constraints throughout this paper.

In general the magnetic field ripple is a good indication of whether a specific configuration is acceptable. It is found here that the ripple can be drastically reduced by carefully shaping and arranging the coils. The zero ripple point can be placed near the center of the torus. Positive ripple can be produced in the inner side of the plasma torus where its effect on confinement is less important. Many configurations are compared under the same constraints. It is found that a staged T-shaped divertor configuration will give the least ripple and current, the best confinement, and smallest physical size. Therefore, it is considered to be the best configuration and is named *cascade bundle divertor*. The detailed confinement characteristics of such a divertor and the engineering implications are studied and discussed later. Specifically the whole divertor assembly is compact and can be installed and removed as a plug-in unit. The coil can be superconducting so that the power loss is negligible.

To study the confinement the computation methods are as follows: MHD equilibrium flux surfaces are obtained for a typical reactor plasma such as INTOR [7]. The flux surfaces are retraced by superimposing the axisymmetric equilibrium surfaces with the divertor coils. Prominent magnetic island structures were observed for the cascade divertor. The thermal particles and impurities are launched on the flux surfaces. Their orbits are tracked using the guiding center equation to the second order of the magnetic moment μ. Collisions and electric fields are included. Many trapping and detrapping occurs along the particle orbit, thereby justifying the diffusive model of transport. In general the thermal conductivity is enhanced by about 40% over axisymmetric neoclassical value. The impurity will diffuse towards the center of the plasma without the divertor when they are launched at a surface halfway between the center and the edge of the plasma. They will diffuse outward when the divertor is turned on.

2. MAGNETICS

The first DITE type bundle divertor consists of two solenoids of constant radius [1]. The field ripple on axis of the plasma is as high as 3% . The ripple will also enhance the diffusion loss [8–12]. All these losses will increase with the number of particles trapped in the ripple, which is in turn proportional to $\sqrt{\epsilon}$, where ϵ is the ripple amplitude. Therefore, the first task is to reduce the ripple. Another serious direct loss is due to the ergodicity of the magnetic surfaces. The second task is to make certain that the magnetic surfaces will not become ergodic when the bundle divertor is added to the system. The third task is to check the confinement of the plasma.

Many coil configurations have been proposed to reduce the ripple or to reduce the current density in the conductor. Nine different configurations have been studied and are illustrated in Fig. 1. All these divertors can be constructed as a single unit and will be called simple divertors. Further improvement with the addition of many auxiliary coils is not the subject of this paper. Figure 1a shows the straight solenoidal coils as of original DITE design. Figure 1b shows the X shaped solenoidal coils, which were proposed to reduce the ripple [13]. This utilizes the fact that the magnetic field drops to zero at a large distance from the X coils. The radius of the solenoids in Fig. 1c is expanding; thus, the current density can be reduced by distributing the turns over larger area [14]. Shown in Fig. 1d are the rectangular shaped coils. Figure 1e shows the coils which are bent into T shape. The horizontal elements of the T coil will increase the field intensity locally; thus, the current and ripple both can be reduced. Figure 1f is a double T shaped divertor. Figure 1g and 1i show the effect of different arrangements of T coils.

Configurations (a) through (d) in Fig. 1 are large size coils. The divertor coils of configurations (e) through (i) are all of same size such that they all are removable as a single unit. Toroidal ripple is defined as $\delta_d = (B_{peak} - B_d)/|B_{peak} + B_d|$ calculated along a field line originated from the centerline of the divertor where B_d is the field at the center line of the divertor. On the inner side of the plasma the field intensity is actually increased for some configurations. Therefore, δ_d can be positive or negative. The ripple on axis for all these configurations is plotted in Fig. 2. The simple straight solenoids have the largest ripple. The X shaped and two reversed T coils are in the middle. The T shaped arrangements give the lowest ripple. The ripple for the T shaped coils

are even negative at the radii less than the major radius. The ripple for the multiple T coils for various sizes all fall in the shaded region. The ripple on axis is reduced by a factor of 4. There is little further reduction by varying the configurations.

For all the configurations other than T shaped coils, the current requirements are very large and the current densities are not practical for engineering consideration. To reduce the current density the coil radius or width has to be increased. This makes the coil maintenance difficult. The double T shaped coils give the best expansion, lowest ripple, and smallest current density. Therefore, the X and reversed T coil configurations can be eliminated from a practical standpoint. A typical toroidal magnetic flux pattern for configuration (h) is shown in Fig. 3. Aside from the reduction in current requirement and ripple, the stagnation axis is concaving towards the plasma instead of concaving towards the divertor like DITE [1] and the mirror ratio is also reduced. These two features will improve the efficiency. The ergodicity of the magnetic surfaces for solenoidal coils with constant radius, expanding radius, and T shaped coils were studied and are now discussed.

To compute the flux surfaces the axisymmetric MHD equilibrium surfaces are superimposed with the perturbed toroidal field. The poloidal flux surfaces are computed by using the PEST code [15] and are shown in Fig. 4. The plasma parameters are that of INTOR $R_o = 5.4$ m, $a = 1.6$ m, $\beta = 6\%$, $q = 2.8$, $I_p = 7.8$MA and $B_o = 5.3$T, which are typical of a power reactor. This was chosen for the purpose of illustrating the engineering feasibility discussed in Section 5. Some care is needed in selecting the poloidal flux configuration for a high β noncircular plasma. For a noncircular high β plasma the flux surfaces are closer together in the area beyond the magnetic axis. The poloidal separatrix is very close to the plasma surface even if it is defined by a limiter or toroidal separatrix. As shown in Fig. 4, the poloidal separatrix is more than 20 cm away, larger than the scrape-off layer, otherwise the poloidal divertor would be competing with the limiter or bundle divertor. On the inner side of the plasma the flux surfaces are less dense and the wall has to be at least 30 cm away; otherwise, the inner wall will become the effective limiter. These are common problems for both bundle divertor and mechanical limiter methods.

The two representative flux surfaces computed at $\phi = 0°$ for configurations e and h are presented in Fig. 5. The fluxes surfaces for single T coils are ergodic. The flux surfaces for

solenoids with expanding radius, double T and triple T are nonergodic. On the $\phi = 0°$ plane, mid-plane of the divertor, the toroidal field is weak; thus, the shear is large. The field lines are moving faster in the poloidal direction, so the line density is reduced. The surface close to the center is $q = 1$; therefore, no surface is traced even after a hundred turns along the torus have been followed. The nonergodic surfaces exhibit island structures. The islands on the surface next to the boundary are large; therefore, further improvement is needed to reduce the island size.

3. CONFINEMENT CHARACTERISTICS

In the previous section we have determined that the cascade T bundle divertor is the optimum configuration. It is not detrimental to the gross confinement since the flux surfaces are nonergodic. In this section we would like to test the microscopic confinement characteristics by following the guiding center orbit of the test particles and study the effect of the ripple on particle diffusion.

Let us first examine the ripple diffusion coefficients. The enhancement of diffusion coefficients due to the toroidal ripple has been discussed by many authors [8–12]. The toroidal ripple has mode number N (equal to the number of TF coils) and the ripple can be represented by sinusoidal function of ϕ. The divertor ripple is 100% at the separatrix. However, the ripple is localized and its magnitude decreases exponentially in both poloidal and toroidal directions. Only one divertor is being considered presently. The effect on the diffusion coefficients due to these two types of ripples is different. To illustrate this difference the ripple plateau particle diffusion coefficient and thermal conductivity are rederived.

The toroidal field due to the presence of toroidal ripple δ_t and divertor ripple δ_d can be written as

$$B = B_o(\psi)\left(1 + 2\epsilon \sin\frac{2\theta}{2} + \delta_t \sin N\phi + \delta_d \exp\frac{-(\phi - \phi_o - \pi/N)^2}{2\alpha}\right). \tag{1}$$

For trapped particles $\mu B_o \simeq mv^2/2$ and in ordinary r,θ,ϕ toroidal coordinates, the radial ripple drift is

$$(v_r)_r = \frac{\rho_\theta v}{2R} N\delta_t \left[\cos(N\phi) - \frac{(q\theta - \pi/N)}{\alpha} \frac{\delta_d}{\delta_t} \exp \frac{-(q\theta - \pi/N)^2}{2\alpha}\right] \tag{2}$$

with $\rho_\theta = v(mc/eB_\theta)^{-1}$ and for $\delta_t > 0$. Following the procedure given in Ref. 10 the ripple diffusion coefficient for $\delta_t > 0$ can be written as

$$D = \left(\frac{\pi}{2}\right)^{1/2} N^2 < \delta_t^2 > \rho_\theta^2 \frac{v_{th}}{R} \frac{B}{B_\phi}\left[1 + \frac{1}{2\pi Nq} < \delta_d^2 > / < \delta_t^2 >\right] \tag{3}$$

for nearly circular flux surfaces, where $< \delta^2 >$ is the averaged value over the flux surface. The thermal conductivity can be written as

$$K = \frac{15}{2}\left(\frac{\pi}{2}\right)^{1/2} nN^2 < \delta_t^2 > \rho_\theta^2 \frac{v_{th}}{R} \frac{B}{B_\phi}\left[1 + \frac{1}{2\pi N^2 q} < \delta_d^2 > / < \delta_t^2 >\right]. \tag{4}$$

At the boundary $\frac{1}{2\pi N^2 q} < \delta_d^2 > / < \delta_t^2 >$ is less than 1. That is, the diffusion due to divertor ripple is enhanced by a factor of less than 1.

The thermal conductivity is also computed numerically using a Monte Carlo guiding center particle orbit code [16] which was modified to include the real coil configuration of the T-shaped divertors and electric field. The guiding center equations, which are accurate to the second order [17], are

$$\underline{V} = \frac{V_\parallel}{B}\left[\underline{B} + \underline{\nabla} \times (\rho_\parallel \underline{B})\right] + \epsilon(0)\,, \tag{5}$$

and

$$\frac{dV_\parallel}{dt} = -\frac{< \mu >}{m} \frac{B_o}{B} \underline{\nabla} B + \frac{q}{m} E_\parallel + 0(\epsilon)\,, \tag{6}$$

and

$$E_{\text{total}} = \frac{m}{2} V_\parallel^2 + \mu B + ze\phi + \frac{m}{2} V_{E\times B}^2 + \int_0^t ze\, E_\parallel\, V_\parallel\, dt\,, \tag{7}$$

where $\rho_\parallel = mV_\parallel/eB$. Particle conservation for these equations of motion is confirmed by the drift kinetic equation $\underline{V} \cdot \underline{\nabla} f = 0$ [18]. The particle pushing algorithm is now briefly described.

A two dimensional spline interpolation is used to compute B and its gradient from the MHD equilibrium flux configurations, and is superimposed on the field and gradient computed from divertor coil geometry. The guiding center is launched in a random velocity direction, keeping toroidal and radial velocity constant. The energy conservation is incorporated in the pushing algorithm directly because guiding center equations conserve energy to at least two orders.

In computing the MHD equilibrium flux surfaces the toroidal field profile used is [15]

$$B_t = B_o R_o \, g, \tag{8}$$

where

$$g = \left[1 - g_p \left(\frac{\psi - \psi_o}{\psi_L - \psi_o}\right)^{\alpha}\right], \tag{9}$$

and the pressure profile used is

$$P = P_o \left(\frac{\psi - \psi_o}{\psi_L - \psi_o}\right)^{\beta}, \tag{10}$$

where ψ_o and ψ_L are fluxes at the magnetic axis and limiter, respectively. P_o is the peak pressure and α, β and g_p are constants. To obtain temperature and density profiles we write

$$\begin{aligned} P &= n_o(\psi) T_o(\psi) \\ &= n_o T_o \left(\frac{\psi - \psi_o}{\psi_L - \psi_o}\right)^{\beta_n} \left(\frac{\psi - \psi_o}{\psi_L - \psi_o}\right)^{\beta_T} \end{aligned} \tag{11}$$

with $\beta_n + \beta_T = \beta$.

To study the interaction of test particles with background plasma the following Coulomb collision terms [16] were included in the ion collisional operator: electron drag, ion drag, ion pitch angle scattering, and ion energy scattering.

The electric fields can be derived from the MHD relationship which gives

$$E_\gamma(\psi) = -\frac{1}{2ne} \vec{\nabla} P \, , \tag{12}$$

and

$$E_\phi(R) = \frac{1}{\sigma} J_\phi(R), \tag{13}$$

where $J_\phi = 2\pi(R^2p' + B_o^2 R_o^2 gg'/\mu_o R)$ and σ is the Spitzer conductivity. The flux in the ripple region is modified according to the form of Eq. (1).

The typical orbits for a 10 keV particle launched at the edge and halfway inside the plasma are shown in Fig. 6. The particle launched near the edge is drifting into the divertor channel as shown by Fig. 6a. Figure 6b shows the orbit of the particle launched in the middle of the plasma and inside the ripple. Figure 6c shows the variation of the phase angle $v_\parallel/v$. The orbit and phase angles oscillate rapidly when the particle is trapped inside the ripple. Banana orbit and phase angle oscillate slowly when it is detrapped. The particle can detrap itself by drifting upward into the lower ripple region above the mid-plane. Collisions and electric field can also change the ripple trapped orbits into banana or circulating orbits, and vice versa. Many trappings and detrappings occur along the particle orbit, thereby justifying the diffusive model of transport.

The real computation time is typically about 10 hours for following 180 particles for 50 ms. Therefore, only one surface has been studied for thermal conductivity. The flux surface chosen is 25% of edge flux and is halfway inside where confinement is more important. The toroidal positions, however, are chosen randomly. The particles are isotropic in velocity space and the velocity directions are random.

The relaxation of the particle distribution as a function of flux at 0.11 ms, 3.3 ms and 11 ms is shown in Fig. 7. The measured thermal conductivity for the tokamak with the optimized divertor is $\chi = 0.29$ which is 40% larger than the axisymmetric neoclassical conductivity $\chi_{NC} = 0.21$. As shown in Fig. 8 a variational study shows that: (1) The thermal conductivity is reduced when the toroidal separatrix is separated form the plasma surface by approximately half the width of the island. This is due to the fact that the separatrix will be outside the island and boundary surface will stay closed. Otherwise the boundary surface will be open and cause large heat leakage across the islands. This suggests that bundle divertors can be used for burn control by changing the separatrix position; (2) The conductivity is reduced when the distance between the divertor and the plasma is increased with height. This is due to the fact that the effect of the fringe field of the divertor is reduced; (3) Because of the higher order multipole effect, the confinement is improved by using more T coils. The choice has to be made based on the trade-off of reasonable

confinement and engineering constraints.

4. IMPURITY TRANSPORT

Several factors must be included in impurity transport calculations. If the impurity is not fully ionized, the line radiation and charge exchange have to be considered. Therefore, oxygen is chosen as the test particle for impurity. The plasma temperature is assumed to be 300 eV in the scrape-off layer. The oxygen is fully ionized. Four cases were studied: The impurity transports inside the plasma and in the scrape-off layer with and without the divertor.

The impurity is launched on the flux surface at 25% of the boundary. As shown by the first column in Fig. 9 and Fig. 10a, the impurity moved to the center of the plasma for axisymmetric tokamak. When the divertor is turned on the impurity diffuses inward as well as outward like the thermal particle shown by the second column in Fig. 9 and Fig. 10b. 12% of the impurity launched has left the plasma. The inward impurity transport in axisymmetric toroidal plasma has been discussed in detail [19–22]. The impurity would diffuse toward the center of the plasma due to the frictional force which is given by

$$F_{zi} = m_{zi}\, n_i\, \nu_{iz}\, (V_{i\theta} - V_{z\theta})\,, \tag{14}$$

and

$$\tilde{V}_{i\theta} = \frac{\nabla P_i|_r}{(ze)\, n_i\, B_\phi}\,, \tag{15}$$

where

$$\nu_{iz} = \frac{2 n_z z^2 e^4 \ln \Lambda}{3(2\pi)^{3/2}\, \epsilon_o^2\, m_{zi}^{1/2}\, (kT)^{3/2}}\,, \tag{16}$$

is the coefficient of friction, $m_{zi} = \frac{m_z m_i}{m_z + m_i}$, $\Lambda = 12\pi(\epsilon_o T_e/e^2)^{3/2}/\sqrt{n_e}$, and ϵ_o is the dielectric constant and the subscripts z and i denote impurity and ion respectively. This frictional force gives rise to an averaged radially inward drifting velocity

$$\tilde{V}_r^J = -\frac{\tilde{F}_{zi}}{n_i z e}\, B_\phi\,. \tag{17}$$

Another inward drifting term is the Ware pinch [23] given by

$$V_r^{E\times B} = \frac{-E_\phi}{B_\theta}. \tag{18}$$

For heavy ions the vertical drift due to field gradient $\frac{\mu}{ze}\frac{B\times\nabla B}{B^2}$ is reduced by a factor of $\bar{z}$ in comparison with a light ion having the same μ, therefore V_r^f and $V_r^{E\times B}$ become the dominant drifts. Since the impurity is confined by the strong electrostatic potential well $ze\phi$ [24] they are driven into the center due to the frictional force and Ware pinch. Since the frictional force is related to E_r through ∇P, there will be no inward diffusion when the electric field is not included as shown in Fig. 11. Taking $T_i = 10$ keV, $n_i = 3\times 10^{20}$ m^{-3} and E_ϕ approximately 0.5 V/m and $B_\theta \simeq 0.5$ T, then the average inward drifting velocities are $V_r^f = -12$ m/s and $V_r^{E\times B} = -1$ m/s. The drift due to friction is 10 times larger than the Ware pinch. The total inward drift is estimated to be 0.6 m in 50 ms which approximately agrees with the Monte Carlo result.

The divertor clearly prevents the impurity from concentrating in the center; instead they diffuse outwardly and are removed by the divertor. The ripple, due to the divertor, is a source for anomalous transport. When the impurity was launched in the scrape-off layer without the divertor, they hardly diffused due to the low temperature at the edge. As shown by Fig. 10c, the impurity diffuses rapidly when the divertor is turned on. Very few of them diffuse into the center of the plasma and most of them are removed by the divertor. At the end of 50 ms of tracking time, only 30% of the impurity launched remains. The impurity transport in the scrape-off layer depends on the temperature. A more detailed study is needed.

5. ENGINEERING FEASIBILITY

As is discussed in the introduction, the most attractive feature of a bundle divertor is its maintainability and the possibility for external cleaning. However, the high current density, large forces, and lack of shielding spaces make the bundle divertor engineering difficult. This section will examine the answer to these problems for the configurations studied. Let us specify the criteria for a feasible divertor. In order to keep the power consumption low the divertor coil has to be superconducting. The reasonable average current density for a stable superconducting coil at 10

T maximum field should be less than 5 k Amp/cm^2 [13]. A commercial Nb_3 Sn cable which can carry 3.5 k Amp/cm^2 is available. Therefore this value is chosen as the current density criterion. In order to protect the insulation material and the superconductor a 60 cm shield of Tungsten and borated water composite is chosen which will give a lifetime of 5 MW years [6]. The forces are not the worst problems. A 100 MN force can be properly handled [14]. However, it should be kept as low as possible. The force is reduced when the current and coil size are reduced and the divertor coils are situated in the weaker toroidal field region. The last criterion allows easy maintenance by means of a plug-in unit.

In this study the width of the divertor is kept smaller than the space between the TF coils as shown in Fig. 3. The outward translational force is about 20 MN. There is 60 cm of shielding space in front of the coils facing the plasma. Therefore these configurations satisfy the engineering criteria as well as giving good confinement. The divertor coil height has been varied from 1.4 m to 2.2 m and the distances from the plasma have been varied from 1.0 m to 1.2 m. The flux surfaces for these cases are all nonergodic and ripple is reasonable. The current increases from 8.75 to 12.3 and 13.55 MA-T when the distance increases from 1.0 m to 1.1 m and 1.2 m. However, the current density can be kept constant by increasing the conductor cross-section proportionally. This demonstrates that a range of designs can be obtained. The choice is a matter of trade-off.

The engineering concept of a cascade bundle divertor and a monolithic bundle divertor assembly are shown in Fig. 12. The divertor assembly is a single unit construction. The forces are transmitted to TF coils through the two horizontal bars and heat stations which are specially designed to minimize the heat leakage and disconnection time. The bars are keyed to the divertor casing and attached to the heat station by a cylindrical bearing. The divertor assembly can be freed and extracted simply by lifting up and dropping down the bars.

6. CONCLUSION

The Monte Carlo modeling of the confinement and impurity transport of a tokamak with a cascade bundle configuration has shown that the thermal conductivity is enhanced only 40% over neoclassical value for axisymmetric plasma and that the divertor will increase the outward impurity

transport. The bundle divertor will screen the impurity. However, the screening effect may depend on the plasma edge temperature and species. A very careful study is needed for designing and carrying out an experiment. A tool for such a study can be developed based on this work.

The study here also shows that the confinement characteristics of a tokamak system with a bundle divertor is strongly influenced by the divertor coil configuration. A wide range of configurations exist which do not cause ergodicity on the flux surfaces in the plasma although magnetic islands are formed due to the ripple.

The toroidal separatrix should not be placed on the boundary determined from MHD equilibrium calculation because of finite island width. The poloidal separatrix should be carefully located outside the scrape-off layer.

The cascade T-shaped configuration represents the best trade-off and can be designed so that the key engineering constraints can be met. Further shape optimization is possible, such as bending the coil toward the plasma and/or situating the coil away from the middle plane. The effect on energetic particles, alpha particle confinement, and on RF heating has to be studied. All this work will be carried out when the computational time of the code is reduced. This code modification is in progress.

ACKNOWLEDGMENTS

Numerous discussions with A. Boozer are acknowledged. The structure concept is the work of J. Tracey. This work is supported by the US Department of Energy under contract No. DE-AC02-78ET-51013.

REFERENCES

[1] Stott, P. E., Wilson, C. M., Gibson, A. *The Bundle Divertor - Part I; Magnetic Configuration*, Nuclear Fusion, 17, 481 (1977).

[2] Stott, P. E., Wilson, C. M., Gibson, A. *The Bundle Divertor - Part II; Plasma Properties*, Nuclear Fusion 184, 475 (1978) and references cited.

[3] Yang, T. F., Callen, J. D., *Stability of the Plasma in a Bundle Divertor*, Nuclear Fusion 20, 1177 (1980).

[4] Harrison, M. F. A., Harbour, P. J., Hatston, E. S., Hughes, M. H., Johnson, P. C., Morgan, J. G., Sanderson, A. D., Spalding, I. J., Thomas, P. R., Walker, A. C., Wooten, A. *A Compilation of Papers Produced by the TIGER Sub-group on Exhaust, Impurity Control and Refueling*, Culham Report CLM-R211, August (1981).

[5] Chang, F. R., Fisher, J. L., *A Supersonic Gas Target for a Bundle Divertor Plasma*, Nuclear Fusion 22, 1003 (1982).

[6] Cheng, E. T. C., Yang, T. F., *The Reflector-Shield Concept for Fusion Reactor Design*, Trans. Am. Nucl. Soc. 34, 49 (1980).

[7] Stacey, W., USINTOR Report, Phase I (1980).

[8] Stringer, T. E. *Effect of the Magnetic Field on Diffusion in Tokamaks*, Nuclear Fusion 12 689 (1972).

[9] Tsang, T., Frieman, E. A., *Toroidal Plasma Rotation in Axisymmetric and Slightly Nonaxisymmetric Systems*, Phys. Fluids 19, 747 (1976).

[10] Boozer, A. H., *Enhanced Transport in Tokamaks due to Toroidal Ripple*, PF 23, 2283 (1980).

[11] Shiang, K. C., Callen, J. D., *Boundary Layer Corrections to Neoclassical Ripple Transport in Tokamaks*, Phys. Fluids, 25 1012 (1982).

[12] P. N. Yushmanov, *Heat Conductivity Due to Banana Orbit Drift in a Magnetic Field with Ripples*, Nuclear Fusion 22, 199 (1982).

[13] Sheffield, J., Dory, R. A., *The Bundle Divertor for Tokamaks*, ORNL-TM6220 March (1978) and USINTOR Report (1979).

[14] Yang, T. F., Lee, A. Y., Ruck, G. W., Prevenslik, T., Smeltzer, G., *Design of an Advanced Bundle Divertor for the Demonstration Tokamak Hybrid Reactor*, IEEE Proc. 8th Symp. On Engr. Probl. of Fusion Res., San Francisco, California (1979).

[15] Johnson, J. L., Dolhed, H. E., Green, J. M., Grimm, R. C., Hsieh, Y. Y., Jardin, S. C., Manickan, J., Okabayashi, M., Storer, R. G., Todd, A. M. M., Voss, D. E., Weiner, K. E., *Numerical Determination of Axisymmetric Toroidal Magnetohydrodynamic Equilibrium*, J. Comp. Physics, 32, 212 (1979).

[16] Potok, R. E. Politzer, P. A., Lidsky, L. M., *Ion Thermal Conductivity in a Helical Toroid*, Phys. Rev. Lett. 20, 1328 (1980). Potok, R. E., Lidsky, L. M., Politzer, P. A., PhD Dissertation, PFC/RR-80-15 (1980).

[17] Northrop, T. G., *The Adiabatic Motion of Charged Particles*, John Wiley and Sons (1963).

[18] Boozer, A. H., Kuo-Petravic, G., *Monte Carlo Evaluation of Transport Coefficients*, P. F. 24, 851 (1981).

[19] Taylor, J. B. *Diffusion of Plasma Ion Across a Magnetic Field*, Phys. Fluids 4, 1142 (1961).

[20] Hirshman, S. P., Sigmar, D. J., *Neoclassical Transport of Impurities in Tokamak Plasmas*, Nuclear Fusion 21, 1079 (1981).

[21] Braginski, S. I. in **Review of Plasma Physics** 1, 205 (1965).

[22] Miyamoto, Kenro in **Plasma Physics for Nuclear Fusion**, MIT Press, 221 (1980).

[23] Ware, A. A. *Pinch-Effect Oscillations in an Unstable Tokamak Plasma*, Phys. Rev. Lett. 25, 916 (1980).

[24] Furth, H. P. Rosenbluth, M. N., IAEA Proc. Third Int'l Conf. on Plasma Phys. and Contr. Nucl. Fusion Research, Novosibirsk, USSR 1, 821 (1968).

FIGURE CAPTIONS

Fig. 1. Divertor coil configurations studied. Configurations (a) through (d) are larger than the space between two adjacent TF coils. Configurations (e) through (i) are smaller than the said space.

Fig. 2. Divertor ripple on axis for the configurations studied. The ripple for multiple T configurations are the lowest. They all fall within the shaded region.

Fig. 3. A typical toroidal magnetic flux pattern computed for the divertor coil configuration in Fig. 1.

Fig. 4. Flux surfaces used in this study. This illustrates that the distance between the plasma boundary defined by the bundle divertor and poloidal separatrix has to be greater than that of the scrape-off layer thickness.

Fig. 5. Magnetic flux surfaces of the tokamak with a bundle divertor. Picture (a) is for configuration Figure 1e and picture (b) is for configuration Figure 1h.

Fig. 6. The orbits of a 10 keV particle launched at the edge and middle of the plasma and inside the ripple. Picture (a) shows that the particle is drifting into the divertor. Picture (b) shows that the particle was first trapped in the ripple and detrapped a fraction of a ms later and became a banana orbit. This effect is further verified by the fluctuation of the phase angle as a function of time in picture (c).

Fig. 7. The relaxation of the test particles in a Maxwellian plasma launched on a surface at $\psi =$ 25% of ψ at separatrix.

Fig. 8. Relative thermal conductivity of a tokamak with a bundle divertor versus radial position and height of the divertor. ΔR_{sep} is the distance of the separatrix from the axisymmetric plasma boundary.

Fig. 9. The diffusion of full ionized oxygen. The oxygen will diffuse toward the center of the plasma 16.5 ms after being launched without a divertor. It diffused outward when the divertor is on. The scales are in units of meters.

Fig. 10. The impurity profiles as a function of flux surfaces at various times. (a) no divertor (b) with divertor and (c) impurity launched in the scrape-off layer. The time sequences corresponding to decreasing amplitudes are indicated in the figure.

Fig. 11. The diffusion of oxygen in axisymmetric toroidal plasma when the electric field is not included. The dashed curve is at 0.11 ms, the solid curve is at 3.3 ms and the solid dot is at 49.5 ms.

Fig. 12. The engineering concept of a plug-in bundle divertor.

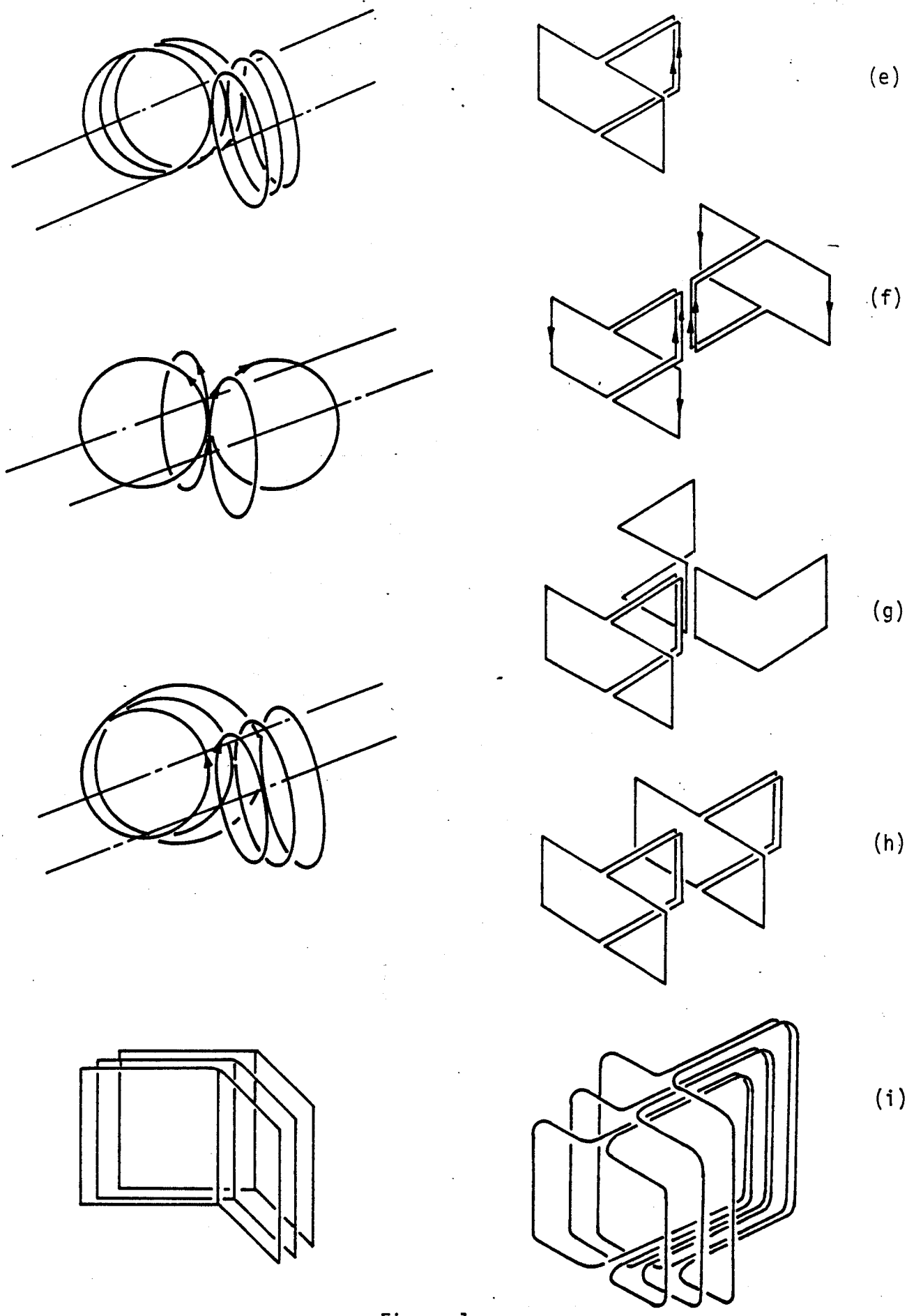

Figure 1

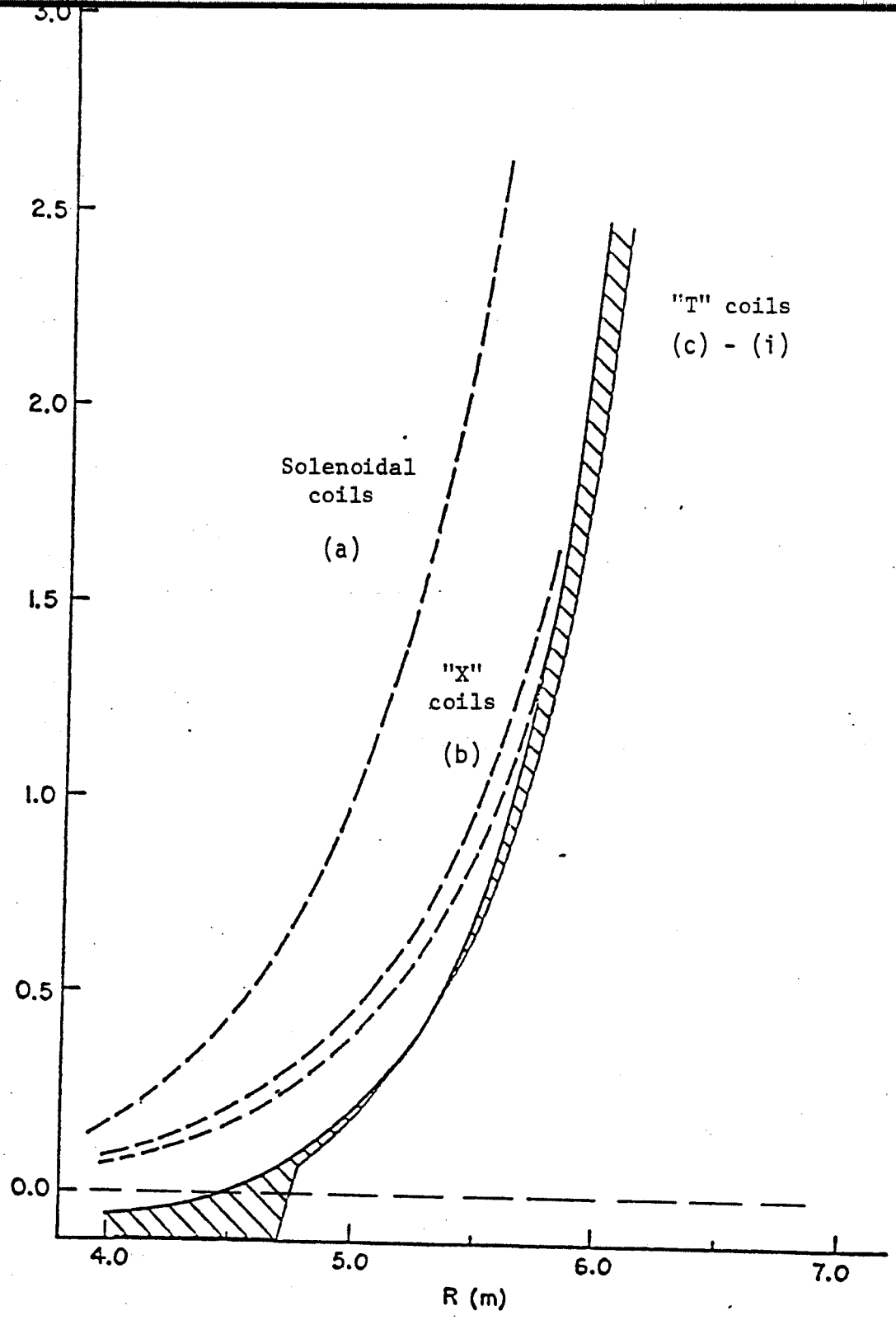
3.0
2.5
2.0
1.5
1.0
0.5
0.0
Solenoidal coils
(a)
"X" coils
(b)
"T" coils
(c) - (i)
4.0
5.0
6.0
7.0
R (m)

Figure 2

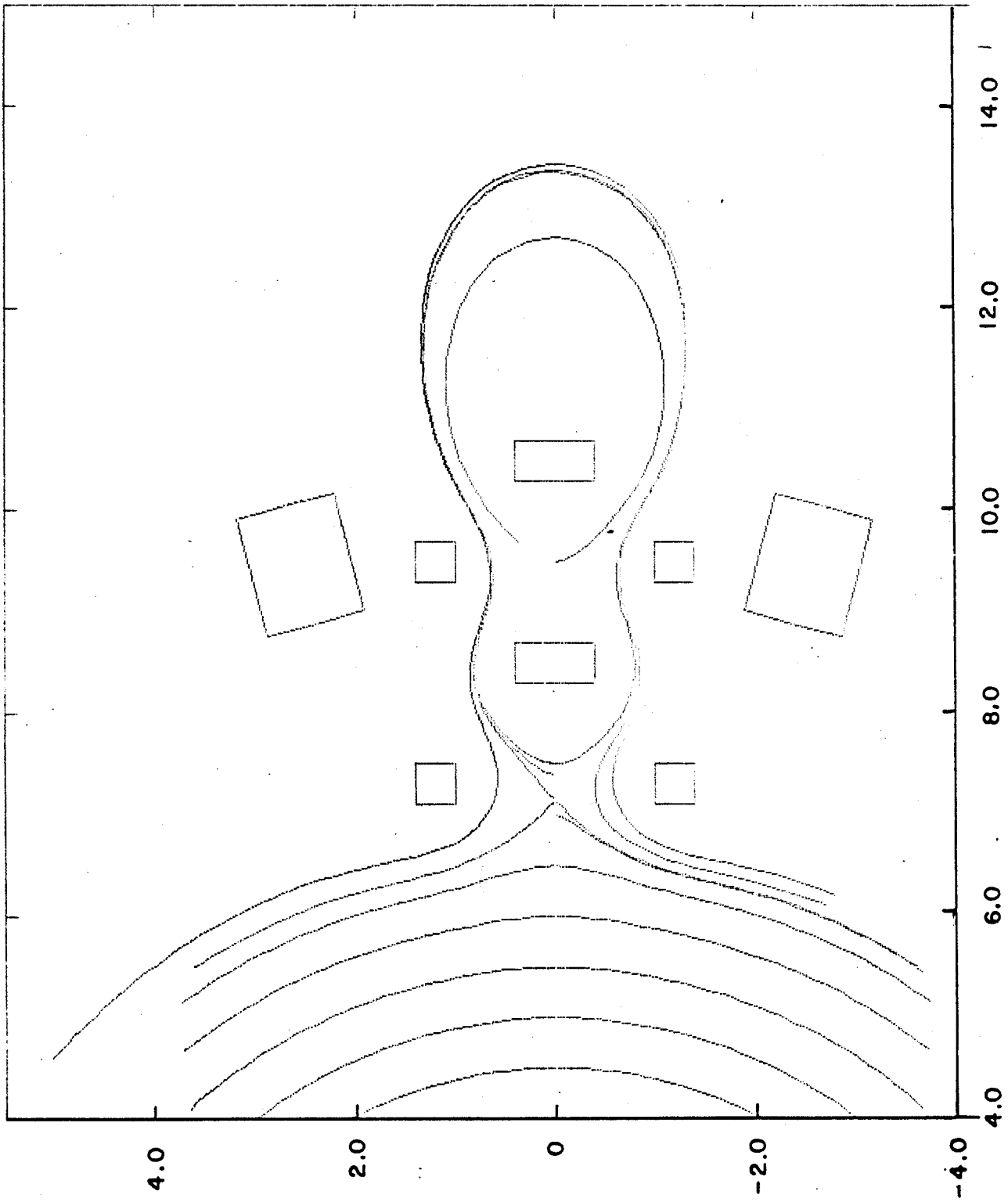

Figure 3

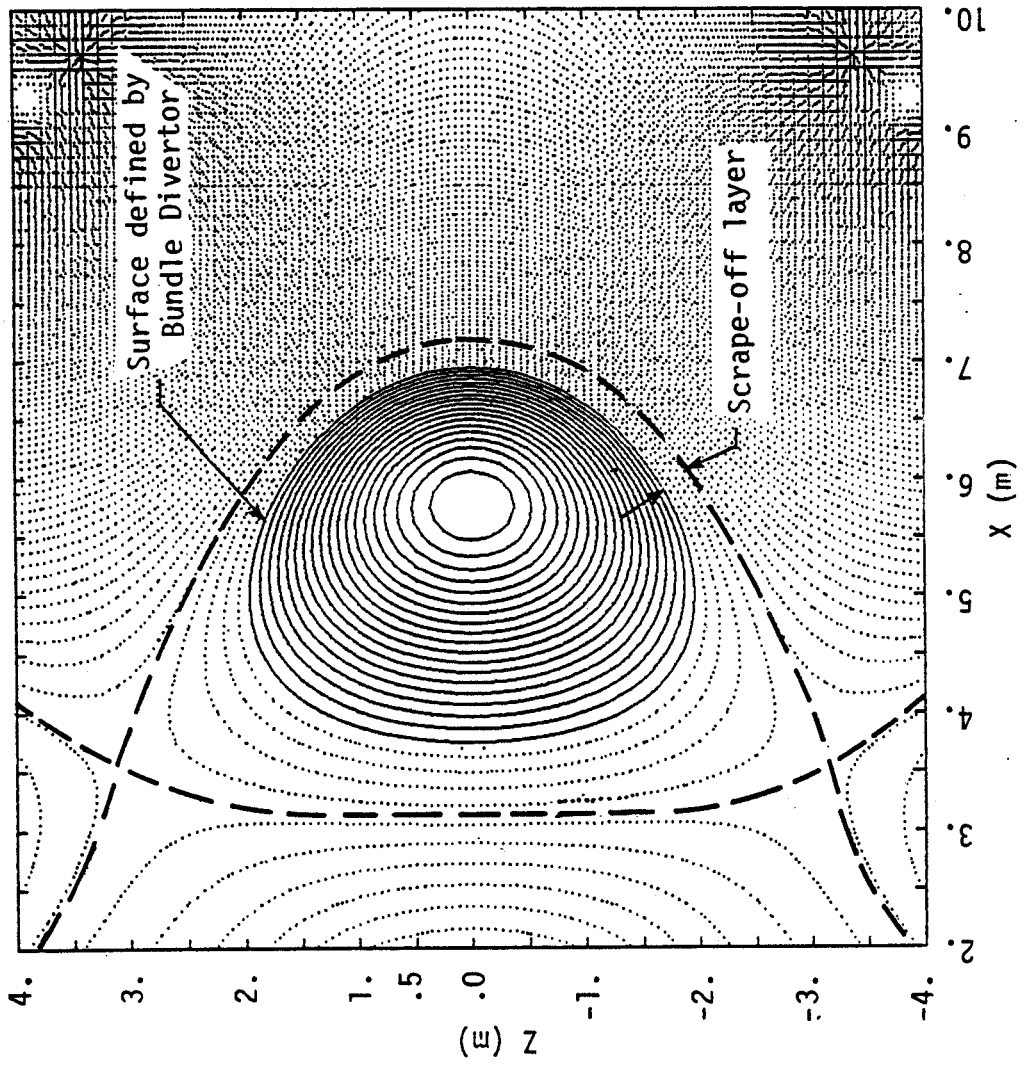
Surface defined by
Bundle Divertor
Scrape-off layer
Z (m)
X (m)
4.
3.
2.
1.
.5
.0
-1.
-2.
-3.
-4.
2.
3.
4.
5.
6.
7.
8.
9.
10.

Figure 4

Figure 5

(a)

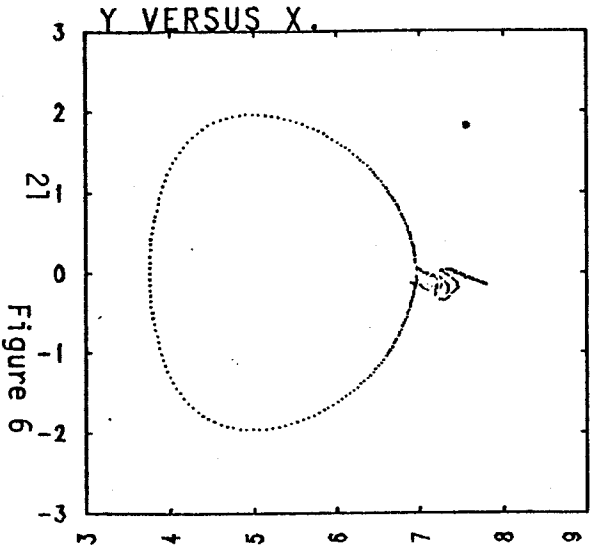
Y VERSUS X.
Z
3
2
1
0
-1
-2
-3
3
4
5
6
7
8
9

(b)

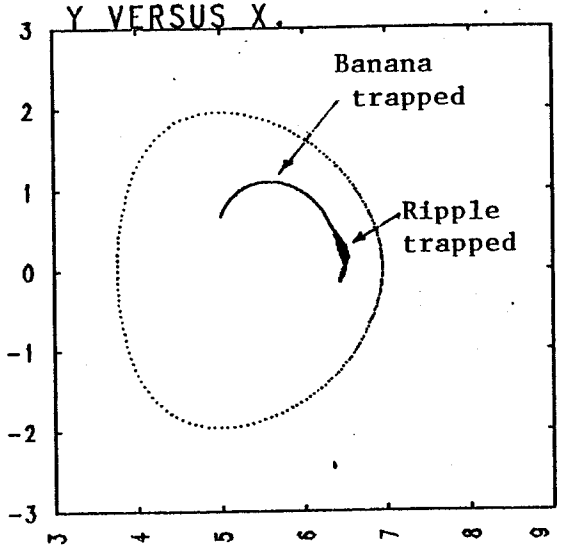
Y VERSUS X.
Banana
trapped
Ripple
trapped
3
2
1
0
-1
-2
-3
3
4
5
6
7
8
9

(c)

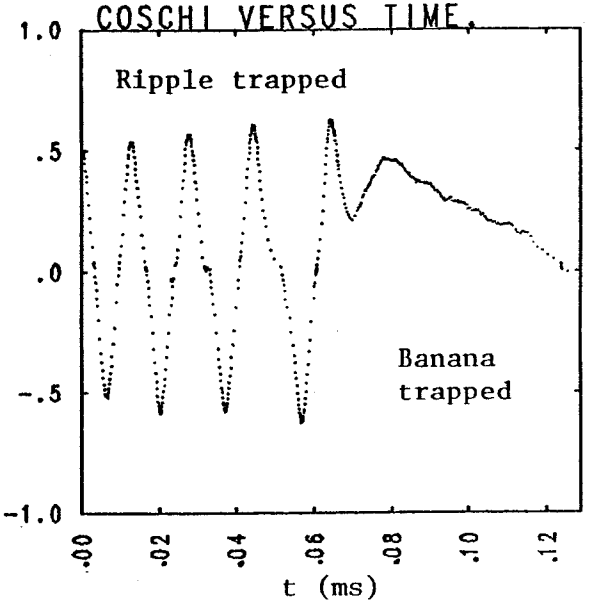
COSCHI VERSUS TIME.
Ripple trapped
Banana
trapped
1.0
.5
.0
-.5
-1.0
.00
.02
.04
.06
.08
.10
.12
t (ms)

Figure 6

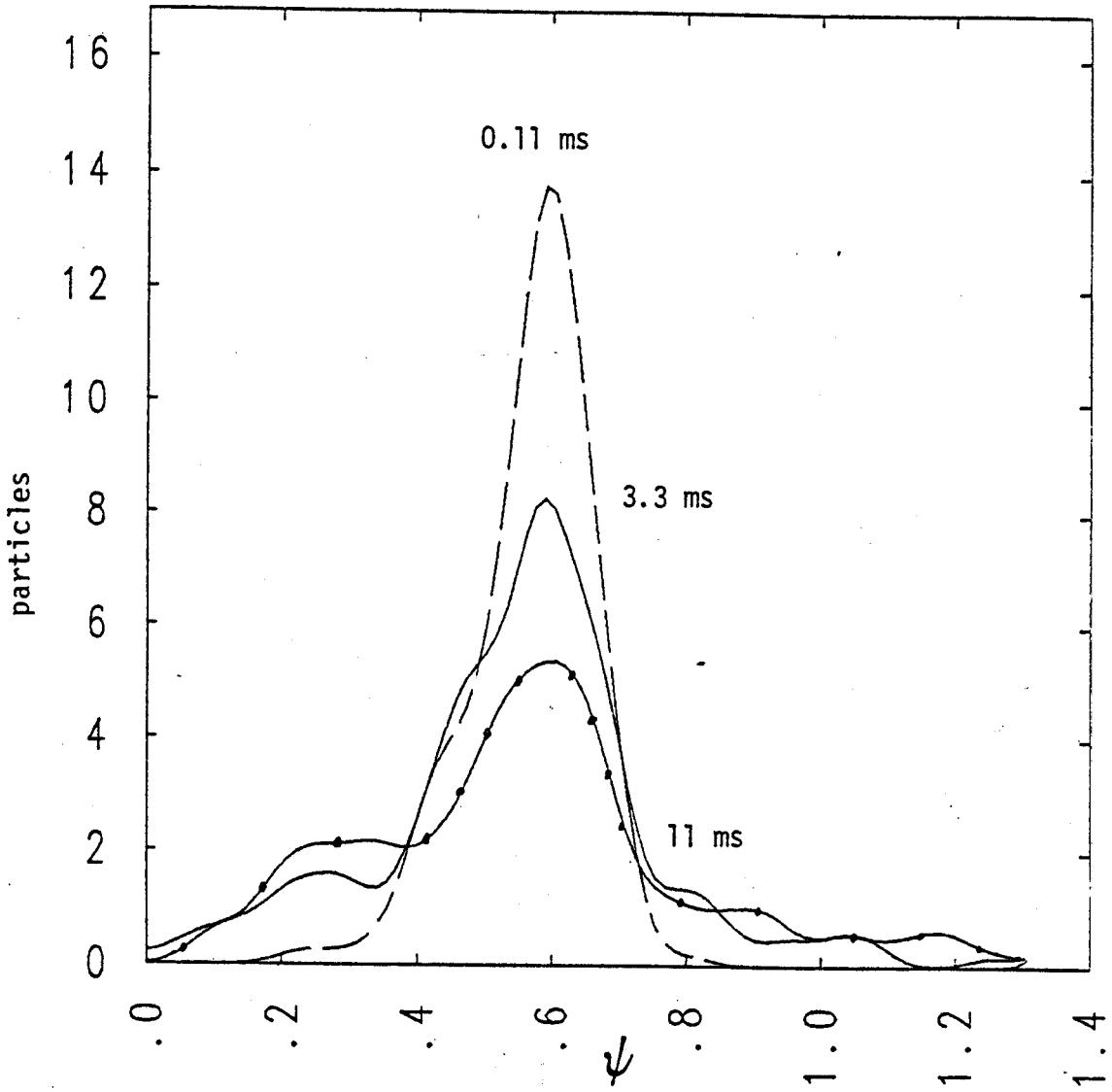

Figure 7

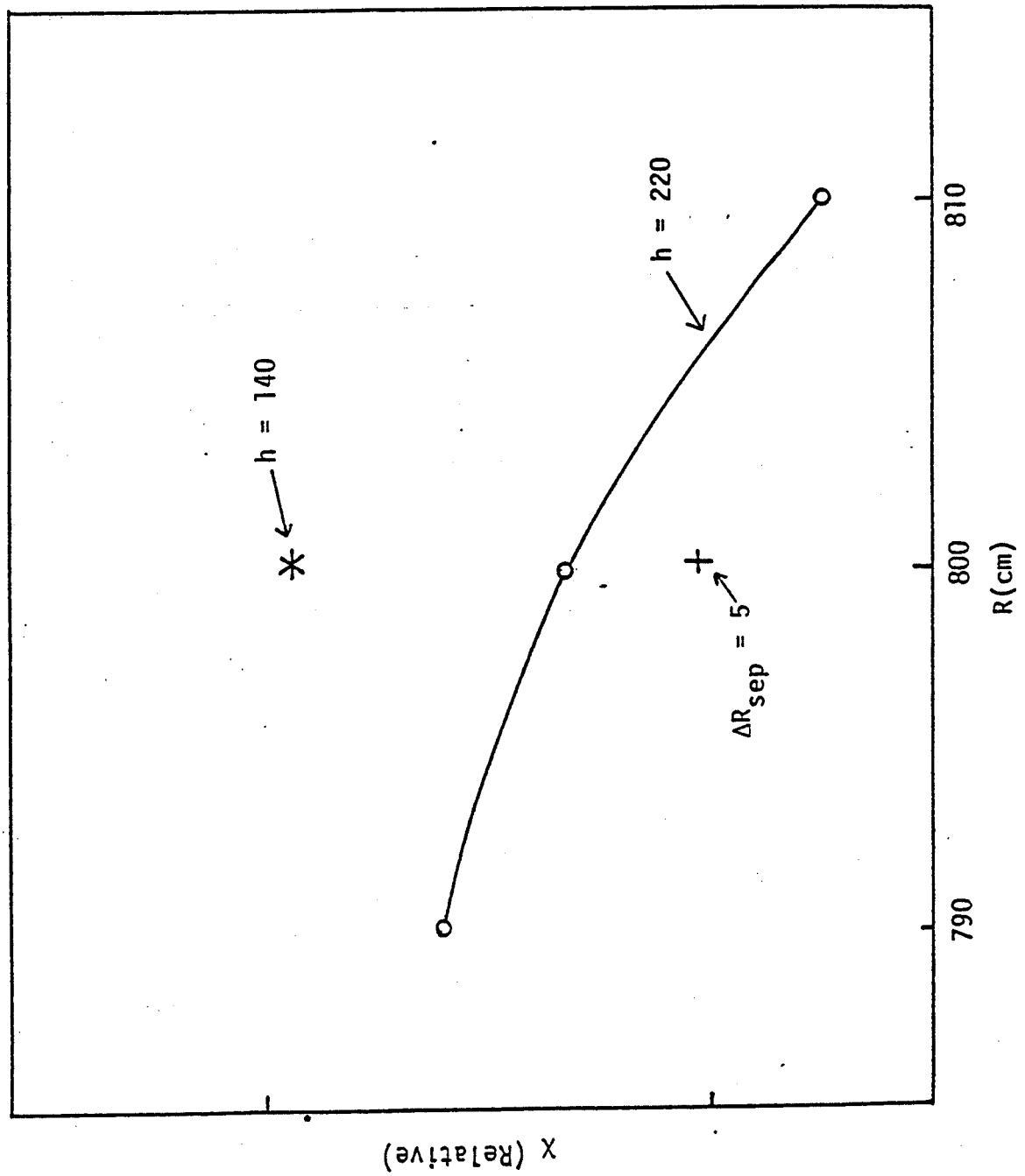

Figure 8

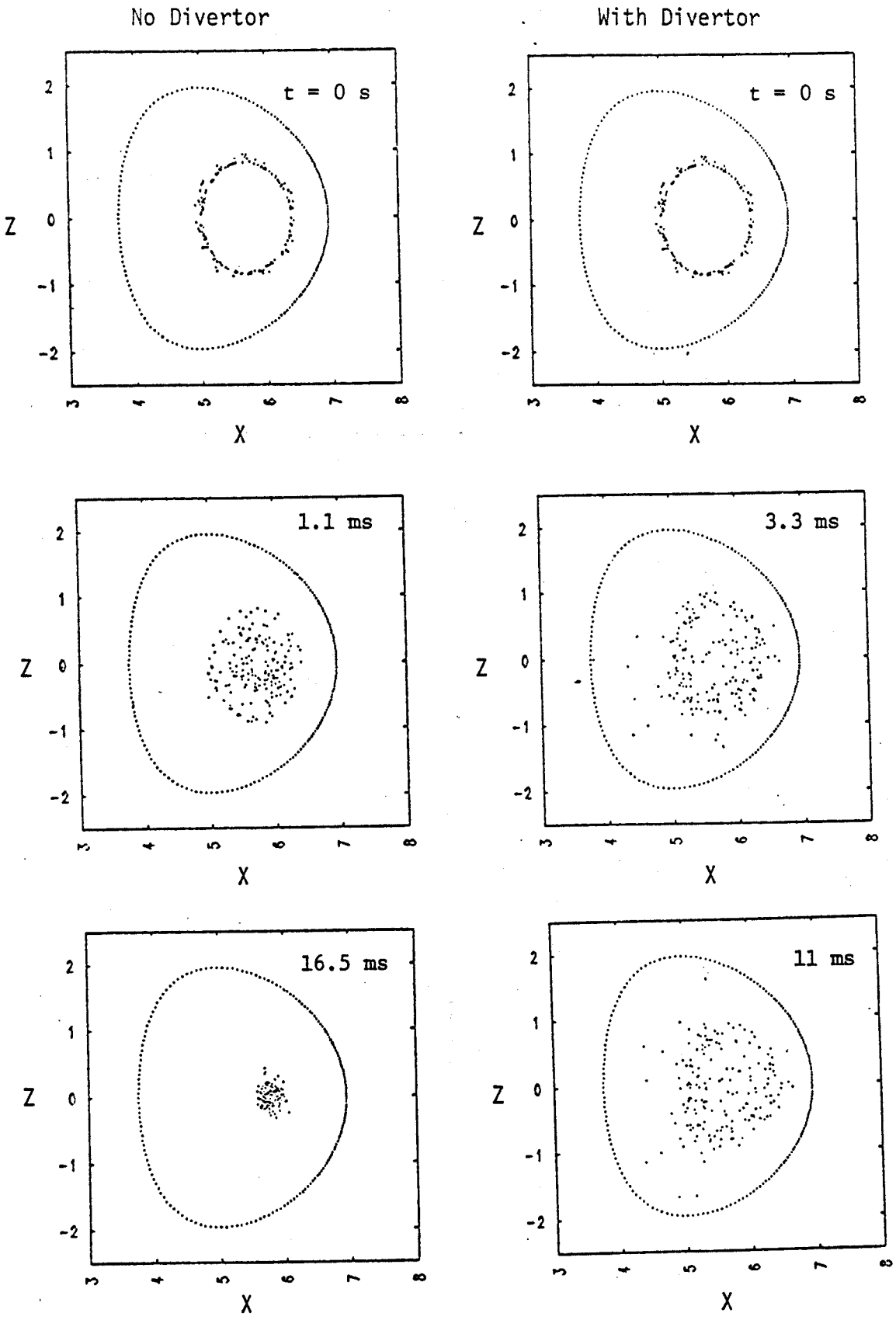

Figure 9

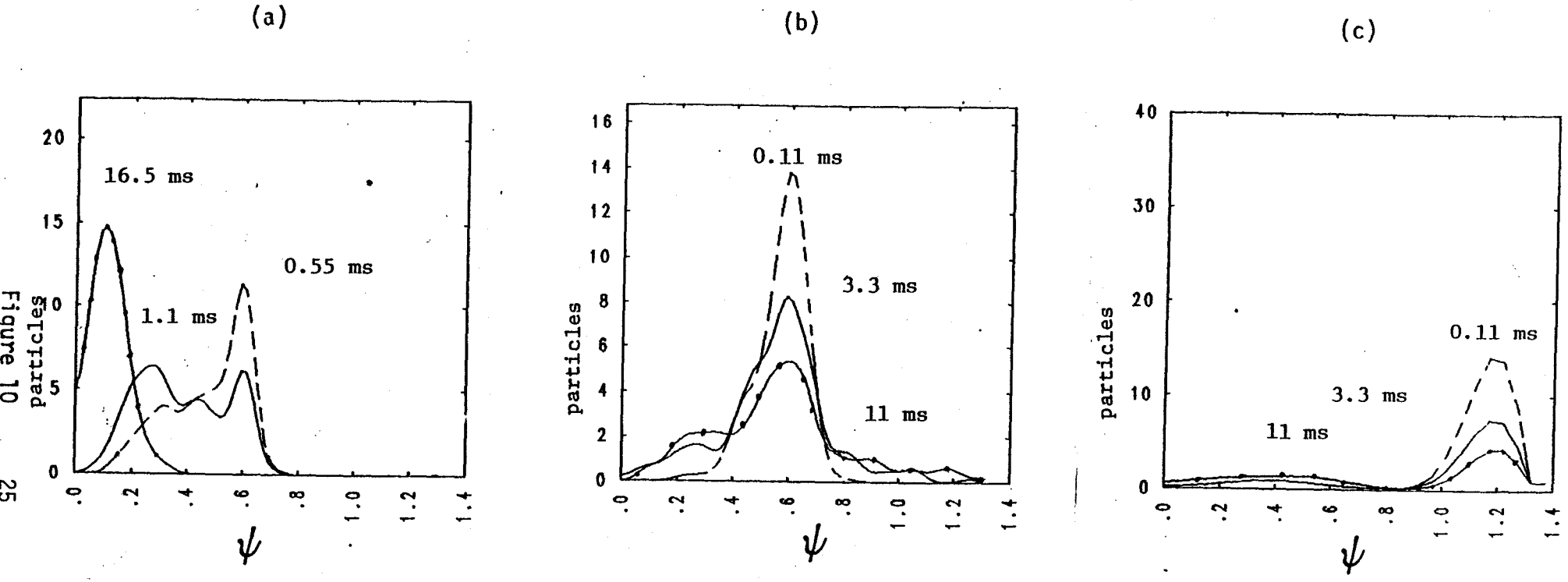
(a)
(b)
(c)
16.5 ms
0.55 ms
1.1 ms
0.11 ms
3.3 ms
11 ms
0.11 ms
3.3 ms
11 ms
particles
ψ

Figure 10

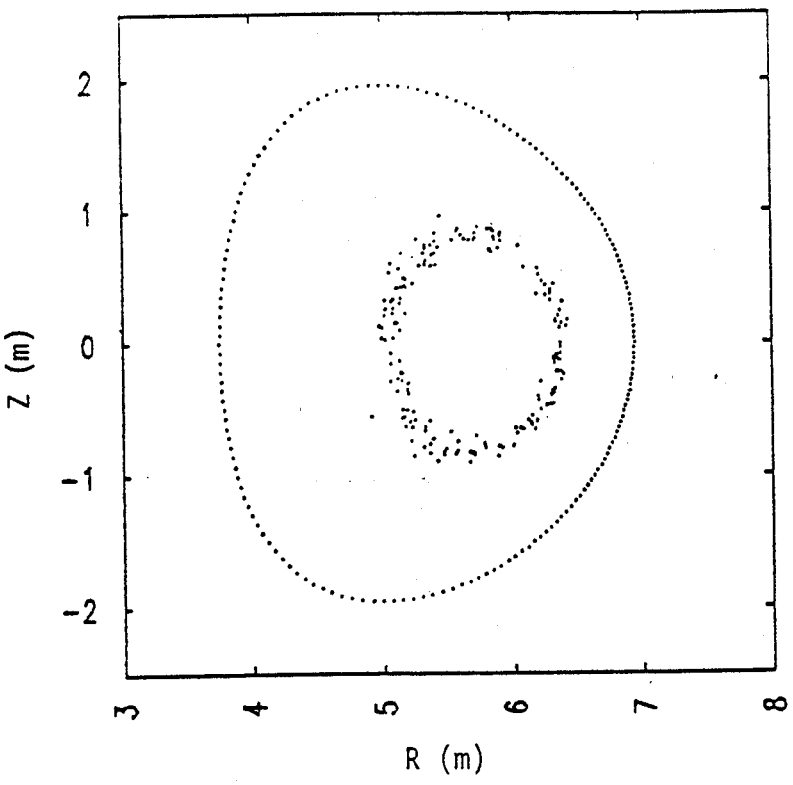

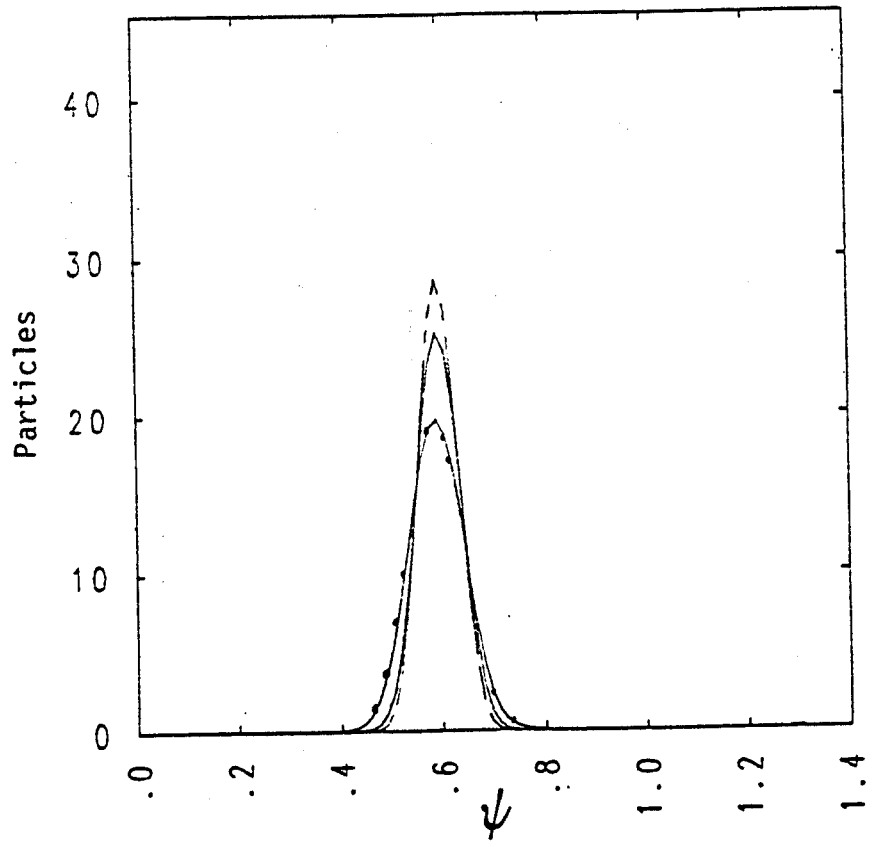

Figure 11

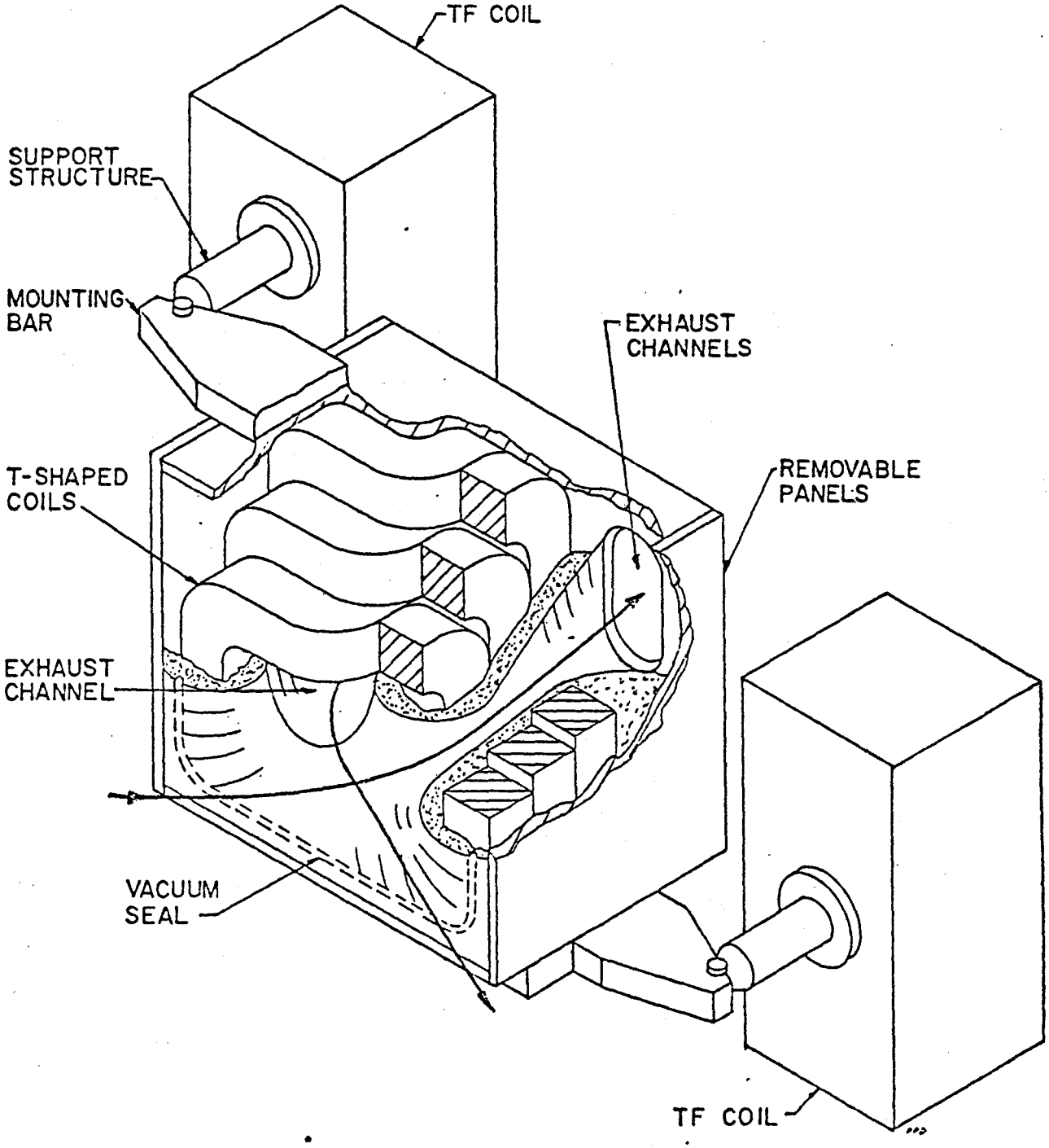
TF COIL
SUPPORT STRUCTURE
MOUNTING BAR
EXHAUST CHANNELS
T-SHAPED COILS
REMOVABLE PANELS
EXHAUST CHANNEL
VACUUM SEAL
TF COIL

Figure 12